FINAL

CONF-851125--3

Prediction of Environmental and Strain-Rate Effects on the Stress Corrosion Cracking of Austenitic Stainless Steels*

by

CONF-851125--3

TI85 012109

P. S. Maiya

ARGONNE NATIONAL LABORATORY
9700 South Cass Avenue
Argonne, Illinois 60439

Materials Science and Technology Division

March 1985

DISCLAIMER

INVITED PAPER to be presented at the Symposium on Predictive Capabilities in Environmentally Assisted Cracking, 1985 Winter Annual Meeting of the American Society of Mechanical Engineers (ASME), Miami, Florida, November 17-21, 1985.

*Work supported by the Office of Nuclear Regulatory Research, U.S. Nuclear Regulatory Commission, Washington, D. C. 20555.

Prediction of Environmental and Strain-Rate Effects on the Stress Corrosion Cracking of Austenitic Stainless Steels*

by

P. S. Maiya

Materials Science and Technology Division
ARGONNE NATIONAL LABORATORY
Argonne, Illinois 60439

ABSTRACT

The stress corrosion cracking (SCC) susceptibility of austenitic stainless steels in high-temperature water is controlled by environmental variables (e.g., dissolved oxygen, corrosion potential, impurities), microstructure (e.g., degree of sensitization), and strain rate. A phenomenological model based on the slip-dissolution mechanism and elastic-plastic fracture mechanics is presented to quantitatively describe the effects of both environment-related parameters and strain rate on SCC in constant extension rate tests. The model predictions are in good agreement with the results of tests performed on Types 304, 316, and 316NG stainless steel at different strain rates in a wide variety of environments relevant to boiling-water reactors.

---

*Work supported by the Office of Nuclear Regulatory Research, U.S. Nuclear Regulatory Commission, Washington, D. C. 20555.

Prediction of Environmental and Strain-Rate Effects on the Stress Corrosion Cracking of Austenitic Stainless Steels*

by

P. S. Maiya

Materials Science and Technology Division
ARGONNE NATIONAL LABORATORY
Argonne, Illinois 60439

I. INTRODUCTION

Constant-extension-rate (CERT) tests have been widely used to determine the stress corrosion cracking (SCC) susceptibility of alloys in aqueous environments.[1-6] The high degree of reproducibility in test results and feasibility of investigating such important variables as strain rate over a wide range of environments have led to quantifiable and interpretable results concerning the SCC susceptibility of materials. Because of the continuing concern over intergranular stress corrosion cracking (IGSCC) in the heat-affected zones of weldments in austenitic stainless steel piping in boiling-water reactors (BWRs), a large number of studies have been focussed on the stainless steel (SS)/water system.[7] These investigations have identified the key parameters affecting IGSCC.

For sensitized conventional materials such as Types 304 and 316 SS, even the high-purity water (with room temperature conductivity $\sigma < 0.2$ μS/cm) used in BWRs is sufficient to facilitate IGSCC because of its content of radiolytically produced dissolved oxygen (~0.2 ppm). It has been shown that IGSCC can be mitigated in sensitized SS by means of hydrogen additions to the feedwater, which result in a lower oxygen content (<0.02 ppm). Impurities (e.g., SO_4^{2-}, NO_3^-, NO_2^-, Cl^-, and CO_3^{2-}) introduced into the recirculating coolant in BWRs as a result of resin intrusion and degradation as well as ion exchange

---

*Work supported by the Office of Nuclear Regulatory Research, U.S. Nuclear Regulatory Commission, Washington, D. C. 20555.

aggravate the IGSCC susceptibility. CERT tests have shown that SO_4^{2-} is one of the most aggressive species, even when present in small quantities ($\leq$0.1 ppm).

From the materials viewpoint, one of the well-recognized contributing factors in IGSCC is the sensitized microstructure (characterized by chromium depletion at the grain boundaries resulting from the precipitation of Cr-rich carbides). Suppression of grain boundary precipitation by lowering of the carbon content below 0.02 wt.% is considered an attractive approach to alleviating the IGSCC problem. The choice of nuclear-grade materials (such as Type 316NG SS with carbon content $\leq$0.02 wt.% and nitrogen levels between 0.06 and 0.1 wt.%) as alternative materials is based upon the above idea. However, despite the expected extreme resistance to IGSCC, Type 316NG SS can become susceptible to TGSCC in impurity environments (impurity levels $\leq$ 0.1 ppm SO_4^{2-} and $\sigma \leq 1$ μS/cm), as shown in CERT tests.

In addition to dissolved oxygen, impurities, and alloy composition and microstructure, the (applied) strain rate $\dot{\varepsilon}$ is recognized as an important parameter in SCC. For example, ductile fracture will occur when the strain rate is high. There exists a critical strain rate $\dot{\varepsilon}$ at or below which SCC occurs.[1] In general, a decrease in the value of $\dot{\varepsilon}$ increases the severity of cracking, although for some alloy systems there exists a lower bound value for $\dot{\varepsilon}$ at which recovery of ductile properties starts to occur. The critical range of strain rates within which environmentally assisted cracking occurs varies from one system to another. If a lower-bound value of $\dot{\varepsilon}$ exists for SS, it is expected to be below 10^{-8} s^{-1}; such a value is difficult to establish in the laboratory. Because of the large number of variables that require study, investigators have presented results obtained on different heats of material under a variety of environmental and loading conditions. It is the objective of this paper to discuss a phenomenological model for interpreting and assimilating the large

body of CERT data on SCC. The approach is based upon the slip-dissolution mechanism[8,9] and elastic-plastic fracture mechanics.[10-12] The model discussed elsewhere[13,14] is reformulated to account for the effects of environment, microstructure or alloy composition, and strain rate (nominal) on SCC. The model is extended to include the relationship between strain rate and average near-crack-tip strain rate, which leads to crack-tip strain rate effects on SCC parameters. The theoretical predictions are compared with the experimental results obtained for Types 316NG, 316, and 304 SS, and an approach to unifying the SCC results obtained for different materials under various environmental and loading conditions is described.

II. MODEL DESCRIPTION

(A) (Nominal) Strain Rate Effects on SCC

Since a detailed description of the model for strain rate effects on SCC has been reported previously,[13] we outline only the essential ingredients. For a fully plastic material containing a crack in a uniform strain field, the crack-tip strain rate is given by

$$\dot{\varepsilon}_T = \frac{\dot{\varepsilon}}{\varepsilon} + \frac{\dot{a}}{a} , \tag{1}$$

where ε and $\dot{\varepsilon}$ are the (nominal) strain and strain rate, respectively, and a and $\dot{a}$ are the crack length and crack growth rate, respectively. Using the slip-dissolution model proposed by Ford,[8,9] one obtains the following relationship between the crack growth rate and the crack-tip strain rate:

$$\dot{a} = A_T \left(\frac{\dot{a}}{a} + \frac{\dot{\varepsilon}}{\varepsilon} \right)^{0.5} , \tag{2}$$

where A_T is a constant. The exact solution of Eq. (2) for CERT tests is

$$a = A_T\sqrt{6t} \ . \tag{3}$$

If one defines $a = a_f$ and $t = t_f$ at failure, Eq. (3) becomes

$$a_f = At_f^{0.5} \ . \tag{4}$$

Equation (4) is not in itself sufficient to determine t_f; an additional fracture criterion is required. In the model, we assume that the failure of the specimen occurs when the J-integral approaches the value J_c, which can be related to ε_f and a_f as follows:

$$J_c = C\varepsilon_f^{n+1}a_f \ , \tag{5}$$

or

$$J_c \simeq C\varepsilon_f a \ , \tag{6}$$

where J_c depends on the material and geometry but is independent of $\dot{\varepsilon}$ and environment, C is a material parameter related to plastic modulus, ε_f is the strain at failure ($\simeq \dot{\varepsilon}t_f$, where t_f is the time to failure), and n is the strain-hardening exponent near fracture (at large strains). Since n has a relatively small value compared to unity, it is ignored for simplicity in Eq. (6). It should be pointed out that higher values of the power law exponent are usually quoted for stainless steel. However, they are based on a description of the stress-strain behavior over a wide range of strains. Equations (4) and (6) can be combined to derive correlations between the SCC (both IGSCC and TGSCC) susceptibility parameters and the strain rate, as follows:[13]

$$\varepsilon_f = (J_c/AC)^{2/3}\ \dot{\varepsilon}^{1/3} \ , \tag{7}$$

$$a_f = A(J_c/AC)^{1/3}\ \dot{\varepsilon}^{-1/3} \ , \tag{8}$$

$$t_f = (J_c/AC)^{2/3}\ \dot{\varepsilon}^{-2/3}\ , \text{ and} \tag{9}$$

$$\dot{a}_{av} = A(AC/J_c)^{1/3}\ \dot{\varepsilon}^{1/3}\ , \tag{10}$$

where $\dot{a}_{av}$ is the average crack growth rate. If one assumes that crack initiation in CERT tests occurs very early in life, $\dot{a}_{av} \simeq a_f/t_f$. It should be noted that Eqs. (7)-(10) are valid only in the critical-strain-rate regime where the severity of cracking increases with a decrease in strain rate. Examination of Eqs. (7)-(9) shows that the fracture-characterizing parameter appears as J_c/C. Hence, from one CERT test at the appropriate $\dot{\varepsilon}$ (that at which SCC susceptibility occurs), both the strain-rate-independent parameters (for a chosen environment and material condition and geometry) A and J_c/C can be determined [see Eqs. (4) and (6)] provided a_f is determined from the fracture surface (t_f and hence $\varepsilon_f \simeq \dot{\varepsilon} t_f$, of course, simply follow from the test). The quantity a_f is usually interpreted as the maximum crack length that can be measured on the fracture surface by means of scanning electron microscopy. A knowledge of the parameters J_c/C and A can then be used to predict the SCC susceptibility at other strain rates [by means of Eqs. (7)-(10)], provided the value of $\dot{\varepsilon}$ lies in the critical-strain-rate regime for the environment and material under investigation.

(B) Crack-Tip Strain Rate Considerations

We have used a J-integral approach to estimate the crack-tip strain rate $\dot{\varepsilon}_T$ [see Eq. (2)] and Ford's slip-dissolution model to relate $\dot{\varepsilon}_T$ to crack growth rate $\dot{a}$. In Eq. (2), A_T is a constant independent of $\dot{\varepsilon}$, but it depends on parameters that control passivation rate, such as degree of sensitization or alloy chemical composition and dissolved oxygen and impurities in the environment. Crack propagation by the slip-dissolution mechanism involves

rupture of the protective oxide (as a result of the attainment of a critical near-crack-tip strain) followed by dissolution of the bared surface. The dissolution of the bare metal surface is assumed to involve mass transport by liquid diffusion. Crack advancement continues until the bare metal is rendered passive again (repassivation). Repassivation is assumed to occur between successive ruptures of the protective oxide at the crack tip. Apart from the fundamental nature of the crack-tip strain rate and related parameters, estimates of crack-tip strain rates $\dot{\varepsilon}_T$ represent a significant step as they allow results obtained with different testing techniques to be correlated by representation on an $\dot{a}$ vs $\dot{\varepsilon}_T$ diagram. The relationships between average near-crack-tip strain rate (which can be estimated from CERT parameters) and the strain rate and other SCC susceptibility parameters of CERT tests can be derived as follows:

An average crack-tip strain rate can be defined by

$$\bar{\dot{\varepsilon}}_T = \frac{1}{t_f - t_o} \int_{t_o}^{t_f} \dot{\varepsilon}_T dt \ . \tag{11}$$

Substituting for $\dot{\varepsilon}_T$ as defined by Eq. (1) and performing the integration, we obtain[13]

$$\bar{\dot{\varepsilon}}_T = \frac{1}{t_f - t_o} \left(\ln \frac{\varepsilon_f}{\varepsilon_o} + \ln \frac{a_f}{a_o} \right) \ , \tag{12}$$

where t_o, ε_o, and a_o are the time, strain, and crack length, respectively, at the initiation of the crack and the subscript f refers to the corresponding values at failure. Assuming that $a_o << a_f$ and $t_o << t_f$ and substituting Eq. (6) in Eq. (12), we obtain

$$\bar{\dot{\varepsilon}}_T = \frac{1}{t_f - t_o} \ln \frac{J_c}{C\varepsilon_o a_o} \quad . \tag{13}$$

By defining

$$K = \ln \frac{J_c}{C\varepsilon_o a_o} \quad , \tag{14}$$

Eq. (13) may be simplified to

$$t_f - t_o = K(\bar{\dot{\varepsilon}}_T)^{-1} \quad . \tag{15}$$

Since K depends only on C (a geometric variable) and J_c (and also on ε_o and a_o), it is assumed to be independent of failure mode (i.e., ICSCC or TGSCC), and it is fairly insensitive to environmental variables. Combining Eqs. (9) (in which t_f is corrected for crack initiation time) and (15), we obtain the following relationship between $\dot{\varepsilon}$ and $\bar{\dot{\varepsilon}}_T$:

$$\dot{\varepsilon} = \frac{(J_c/AC)}{K^{3/2}} (\bar{\dot{\varepsilon}}_T)^{3/2} \quad . \tag{16}$$

Since A is strongly dependent on the environment, the relation between $\dot{\varepsilon}$ and $\bar{\dot{\varepsilon}}_T$ is not solely dependent on geometry and mechanics. Combining Eqs. (10) and (16) gives the following relationship between $\bar{\dot{a}}_{av}$ and $\bar{\dot{\varepsilon}}_T$:

$$\dot{a}_{av} = \frac{A}{K^{\frac{1}{2}}} \bar{\dot{\varepsilon}}_T^{0.5} \quad . \tag{17}$$

Equation (17) is identical in form to the power law relationship proposed by Ford in his slip-dissolution model[9] but is expressed in a form that can be verified in CERT tests. Thus the consistency of CERT test results with the slip-dissolution model of Ford can be examined.

A relation similar to Eq. (17) has been used by Garud and Gerber[15] with the assumption that the crack-tip strain rate can be approximated by the nominal strain rate.

(C) Environmental Effects

In the preceding sections, we described the model for strain rate effects on susceptibility to SCC. Though it is not explicitly evident, Eqs. (7)-(10), which relate the SCC susceptibility parameters of the CERT tests to strain rate, embody the environmental (as well as material-related) effects on SCC as well. This can be seen by representing the correlations in a generalized form:

$$P = A^p \left(\frac{J_c}{C}\right)^q (\dot{\varepsilon})^r \qquad (18)$$

where

P = SCC susceptibility parameter (e.g., ε_f, a_f, t_f or $\dot{a}_{av}$),

A = function of dissolved oxygen or corrosion potential and chemical composition of the alloy and microstructure ($= a_f/t_f^{0.5}$),

J_c/C = fracture-characterizing parameter (defined earlier) which depends on the geometry and material but is independent of environment,

and p, q, and r are given by the model. For a fixed strain rate, assuming that one of the environmental variables (e.g., dissolved oxygen or corrosion potential) dominates SCC behavior and other variables are not important or are held constant. Eqs. (7)-(9) can be rewritten in the following manner to highlight the environmental effects on SCC and to facilitate more direct experimental verification:

$$a_f = \left(\frac{J_c}{C\dot{\varepsilon}}\right)^{1/3} A^{2/3} , \tag{19}$$

$$t_f = \left(\frac{J_c}{C\dot{\varepsilon}}\right)^{2/3} A^{-2/3} , \tag{20}$$

$$\dot{a}_{av} = \left(\frac{J_c}{C\dot{\varepsilon}}\right)^{-1/3} A^{4/3} , \tag{21}$$

and

$$\varepsilon_f = \left(\frac{J_c \dot{\varepsilon}^{\frac{1}{2}}}{C}\right)^{2/3} A^{-2/3} . \tag{22}$$

The above formalism enables one to extrapolate the SCC behavior from one strain rate to another (in the critical-strain-rate regime) in a given environment. It is also possible to extrapolate or interpolate from one set of environmental conditions to another provided the dependence of A on those environmental variables can be established in a quantitative fashion.

III. COMPARISON BETWEEN THEORETICAL PREDICTIONS AND EXPERIMENTAL RESULTS

A significant amount of experimental information has been obtained in the present program for Types 316NG, 316, and 304 SS in high-temperature water without impurities ($\sigma < 0.2$ μS/cm) and with SO_4^{2-} as an impurity ($\sigma \simeq 0.9$ μS/cm). For Types 316NG and 316 SS, the effects of strain rate on SCC have been systematically studied.[16] For Type 304 SS, the effects of dissolved oxygen, hydrogen, and sulfate in the water at low concentrations have been investigated in detail by W. E. Ruther et al.[17] at one strain rate. Thus, by using the two sets of results obtained for the three types of stainless steel, both the strain-rate and environmental effects on SCC susceptibility can be examined in

terms of the model described in the previous section. The chemical composition of the three materials is shown in Table I.

Cylindrical tensile specimens (6.35-mm diam and 36.0-mm gauge length) of Types 316NG and 316 SS were solution annealed for 0.5 h at 1050°C and aged for 24 h at 650°C. This heat treatment produced no measurable degree of sensitization in Type 316NG SS, as assessed by the electrochemical potentiokinetic reactivation (EPR) method,[18] but did produce sensitization in Type 316 SS (EPR $\simeq$ 17 C/cm^2). This observation is also consistent with microstructural observations by transmission electron microscopy, which showed the presence and absence of Cr-rich carbide precipitates at the grain boundaries of Types 316 and 316NG SS, respectively.

The details of the heat treatment and specimen preparation and testing procedures have been described elsewhere.[13,17] Briefly, the specimen was enclosed in an autoclave wich a once-through water system and exposed to water with controlled amounts of dissolved oxygen ($\sim$0.2 ppm) and SO_4^{2-} impurity (0.1 ppm) at a temperature of 289°C, a pressure of 9.0 MPa (1300 psi), and a flow rate of 8.1 cm^3/min. Tests were conducted in CERT systems with a worm gear Jactuator, a gear reducer, and a variable-speed motor drive mechanism. The strain rates of specimens varied between 10^{-8} and 10^{-5} s^{-1}. The strain rate of the specimens in the CERT systems as a function of motor speed was calibrated by direct measurements of the strain on sample specimens; an axial extensometer was used. After the tests were completed, the fracture surfaces were examined by scanning electron microscopy to determine the maximum intergranular or transgranular crack length. The average crack growth rates $\dot{a}_{av}$ were estimated with the assumption that the crack length and strain at crack initiation are small compared to values at failure. The results discussed in this study are not significantly affected by the choice of crack initiation parameters over a wide range of values.

The effects of dissolved oxygen, hydrogen, and sulfate in the water for Type 304 SS sensitized to EPR values of 2-30 C/cm^2 have been investigated by W. E. Ruther et al.[17] at a strain rate of 1×10^{-6} s^{-1}. The specimen preparation, experimental procedure, and CERT system used in their study are similar to those used for Types 316NG and 316 SS. In their study, to better characterize the environment, steady-state open-circuit electrochemical potentials relative to an external 0.1M KCl/AgCl/Ag reference electrode were measured at 289°C. The measured potentials were converted to the standard hydrogen electrode by using the thermocell and thermal liquid junction potentials for 289°C. As can be seen from Fig. 1, the dissolved-oxygen concentration has a significant effect on Type 304 SS potential and the plot of corrosion potential as a function of log $[O_2]$ exhibits a characteristic "S" shape. These investigators also observed that the plot of log $(\dot{a}_{av})$ of Type 304 SS as a function of log $[O_2]$ exhibits a similar trend, with a transition in the "S" curve corresponding to a change in the SCC mode from IGSCC to TGSCC. The results obtained on strain rate and oxygen potential effects on SCC are examined below in terms of the model predictions.

(A) Strain Rate Effects

The relationship between a_f and t_f derived in the model [Eq. (4)] can be verified by CERT test results. The experimental results observed for IGSCC in Type 316 SS and TGSCC in 316NG SS in an impurity environment over a range of strain rates (Fig. 2) show the predicted relationship. Figure 2 shows the log-log plots of a_f vs $(t_f - t_o)$ for the two materials in an impurity environment (where t_o corresponds to ~1% strain from the start of the test). It is important to point out that the agreement between the prediction and experimental results, though consistent with the slip-dissolution model, is not

in itself sufficient to separate the two mechanisms (e.g., slip-dissolution vs hydrogen embrittlement) that may be operating in SCC.

In the log-log plot of Fig. 3, the linear relationship between a_f and ε_f is observed for Types 316NG and 316 SS in two different environments. From this slope (-1.12), based on Eq. (5), the strain-hardening coefficient n is 0.12. This value, of course, is in agreement with the value expected for SS at large plastic strains and hence justifies the use of Eq. (6) (where n is negligible compared to unity) in deriving correlations between the SCC susceptibility parameters and $\dot{\varepsilon}$. In Fig. 3, the data for Types 316NG and 316 SS in two environments have been combined, since the fracture-characterizing parameter J_c (or more specifically J_c/C) is approximately the same for the two materials and independent of the environment.

Because both relations [Eqs. (4) and (6)] are obeyed by the experimental results, we expect the results on SCC to behave in accordance with the power-law relations described in Eqs. (7)-(10). Log-log plots of t_f and $\dot{a}_{av}$ as functions of $\dot{\varepsilon}$, shown in Figs. 4 and 5, respectively, yield straight lines with slopes that are consistent with the strain rate exponents predicted by Eqs. (9) and (10), respectively. Figure 5 also shows the relative SCC susceptibility of the two materials, namely, the average transgranular crack growth rates in Type 316NG SS are slower than the average intergranular crack growth rates by a factor of $\sim$3 over a range of strain rates. These correlations are useful in predicting the severity of SCC when the strain rate is lowered in a test. For IGSCC, it has been shown that from the CERT test results obtained at a higher $\dot{\varepsilon}$ of $\geq 1 \times 10^{-6}$ s^{-1}, the IGSCC susceptibility at a lower $\dot{\varepsilon}$ ($\sim 10^{-7}$ s^{-1}) can be predicted accurately[14] provided the value of the lower $\dot{\varepsilon}$ is in the critical-strain-rate regime (see Fig. 6). Thus the model may be useful for extrapolation to an even slower $\dot{\varepsilon}$, $\sim 10^{-8}$ s^{-1}, which is closer to the rates encountered in

service (although the stresses and strains in CERT tests are considerably higher). This is possible provided processes such as crack blunting, which retard the crack growth, are not operating. Recently, a slow-strain-rate test conducted on Type 316NG SS at $\dot{\varepsilon} = 5 \times 10^{-8}$ s^{-1} showed that TGSCC occurred with an $\dot{a}_{av}$ which was roughly a factor of two lower than the value obtained from Fig. 5 by means of extrapolation. Thus, the model appears to give conservative estimates of the crack growth rates in the very-slow strain-rate regime.

(B) Crack-Tip Strain Rate Effects

The average near-crack-tip strain rate $\bar{\dot{\varepsilon}}_T$ estimated from CERT test results and Eq. (17) is plotted vs $\dot{a}_{av}$ for Types 316NG SS and 316 SS in Fig. 7. The results show that $\dot{a}_{av}$ varies as the square root of $\bar{\dot{\varepsilon}}_T$, as predicted by the model. These results are consistent with Ford's model, which relates the two in terms of instantaneous quantities rather than in terms of average parameters as has been done here. Formulation of Ford's slip-dissolution model for CERT tests in terms of average quantities makes it amenable to experimental verification. The applicability of the model to results obtained in a wide variety of environments can also be demonstrated. The estimation of crack-tip strain rates in CERT tests provides a link for correlating the results with the crack growth data obtained under different testing conditions. At present, our ability to do this is hampered by the difficulty of obtaining estimates of the appropriate crack-tip strain rate for different types of loading including the conventional fracture mechanics tests.

(C) Environmental Effects

Extensive CERT test results have been obtained in environments with a wide range of dissolved-oxygen concentrations (from 8 to less than 0.02 ppm),[17,19] including high-purity water ($\sigma \leq 0.2$ μS/cm) and impurity environments

containing 0.1 ppm SO_4^{2-} ($\sigma \lesssim 0.9$ μS/cm). From the data, the crack growth rate constant A [see Eq. (4)] has been calculated from a_f and t_f on the basis of the same assumptions as before with regard to crack initiation. Log-log plots of $\dot{a}_{av}$ vs A have been constructed to see whether the data can be described by the model [Eqs. (19)-(22)]. Figure 8 shows the results in high-purity water for Type 304 SS sensitized to EPR = 2 C/cm^2 and EPR = 20 C/cm^2; these results are in satisfactory agreement with Eq. (21). The results for sensitized Type 304 SS in the impurity environment (Fig. 9) show similar agreement with the model (taking experimental scatter into account). In both high-purity and impurity environments, the model describing the variation of $\dot{a}_{av}$ with A shows that once the material is sensitized, the degree of sensitization has a relatively small effect on SCC. The dissolved oxygen or steady-state open-circuit corrosion potential has a dominant effect in controlling the SCC behavior. These results are relevant to the hydrogen water chemistry that is being considered for use in some BWRs to control the SCC problem. Variation of other SCC parameters such as a_f, t_f and ϵ_f with A is also found to be consistent with the model. If we can determine, in an analytical fashion, the dependence of A on environment-related variables such as dissolved oxygen content (or corrosion potential) and impurities, the model can be used to interpolate or extrapolate the SCC susceptibility from one environment to another for a given material. This will be attempted in future work.

Because of the considerable improvements in material performance that can be derived from a reduction in the dissolved-oxygen content in water, similar experiments have been conducted for Type 316NG SS. In conjunction with the better resistance to SCC of Type 316NG SS, the use of hydrogen chemistry can

only result in further improvement. For the nuclear-grade material, dissolved oxygen was varied (without the use of H_2) by using nitrogen cover gas with controlled oxygen content. The oxygen content was varied from 8 to 0.02 ppm; the resultant corrosion potentials encompass both the approximate upper- and lower-bound values encountered under various BWR operating conditions. The results for Type 304 SS were obtained[19] at $\dot{\varepsilon} = 1 \times 10^{-6}$ s^{-1}. Because of the better resistance to SCC of Type 316NG SS, the results for that material were generated at a slower $\dot{\varepsilon}$ of 2×10^{-7} s^{-1}. The model was then used to determine the relative SCC susceptibility of the two materials at $\dot{\varepsilon} = 2 \times 10^{-7}$ s^{-1} (Fig. 10). The shapes of the curves for the two materials show similar trends regardless of the failure mode (IGSCC or TGSCC). The results of the analysis show that for Type 304 SS, $\dot{a}_{av}$ decreases by a factor of about 8 for dissolved-oxygen concentrations in the range from 8 to 0.02 ppm or less. For Type 316NG SS, $\dot{a}_{av}$ decreases by a factor of 4 -- a smaller decrease, but still significant. The estimated relative SCC susceptibility of the two materials is being confirmed by experiments on Type 304 SS at a strain rate of 2×10^{-7} s^{-1}.

Finally, it should be pointed out that the phenomenological model for strain-rate and environmental effects on SCC in the critical-strain-rate regime discussed in this study is based on approximations that are difficult to justify a priori for the large plastic deformations that occur in CERT tests. For example, a J-based approach is used to characterize the crack growth behavior as well as fracture in the fully plastic material. Secondary cracking which may occur at large plastic strains during slow straining in an aggressive environment has been ignored. However, the results on the value of the strain-hardening exponent determined from the fracture criterion (see Fig. 3) and the good agreement between the model predictions and experimental results over a wide range of material, strain rate, and environmental variables all indicate

that the approximations of the model are reasonable. In future work, we will attempt to relate the SCC susceptibility results obtained in CERT tests to those obtained under different loading histories and to correlate the laboratory data with those obtained under service conditions.

IV. SUMMARY

A phenomenological model for quantitatively describing the effects of strain rate, environment, and alloy microstructure on SCC susceptibility in slow-strain-rate tests is discussed. Basically, the theoretical description makes use of a J-integral approach to estimate the crack-tip strain rate and to determine the fracture in a fully plastic material. These results, in conjunction with the slip-dissolution model of Ford, are used to derive the crack growth behavior and correlations between the SCC susceptibility parameters and strain-rate-, material-, and environment-dependent variables in an explicit manner. The theoretical predictions are shown to be in good agreement with the experimental results on SCC (both IGSCC and TGSCC) for Types 316NG, 316 and 304 SS. An extension of the phenomenological approach is used to derive Ford's slip-dissolution model in terms of measurable average quantities in CERT tests rather than in terms of instantaneous quantities, which are difficult to measure or estimate. The capabilities of the model to provide reliable means extrapolations from high-strain-rate to slow-strain-rate regimes in various environments and from one environment to another at various strain rates have been examined.

ACKNOWLEDGMENTS

I wish to thank W. J. Shack and T. F. Kassner for helpful discussions.

REFERENCES

1. Parkins, R. N., "Development of Strain-Rate Testing and Its Implications," Stress Corrosion Cracking: Slow Strain Rate Technique, ASTM STP 665, ASTM, Philadelphia, 1979, pp. 5-25.
2. Takaku, Hiroshi. Tokiwai, Moriyasu, and Hirano, Hideo, "Effects of Cyclic Tensile Loading on Stress Corrosion Cracking Susceptibility for Sensitized Type 304 Stainless Steel in 290 C High Purity Water," Corrosion, Vol. 35, No. 11, 1979, pp. 523-531.
3. Tokano, Michinori, "Effect of Strain Rate on Stress Corrosion Cracking of Austenitic Stainless Steel in $MgCl_2$ Solutions," Corrosion, Vol. 30, No. 12, 1974, pp. 441-446.
4. Wearmouth, W. R., Dean, G. P., and Parkins, R. N., "Role of Stress in the Stress Corrosion Cracking of Mg-Al Alloy," Corrosion, Vol. 29, No. 6, 1973, pp. 251-258.
5. Ford, F. P., and Povich, M. J., "The Effect of Oxygen Temperature Combinations on the Stress Corrosion Susceptibility of Sensitized Type 304 Stainless Steel in High Purity Water," Corrosion, Vol. 35, No. 12, 1979, pp. 569-574.
6. Powell, D. T., and Scully, J. C., "Stress Corrosion Cracking of Alpha Titanium Alloys at Room Temperature," Corrosion, Vol. 24, No. 6, 1968, pp. 151-158.
7. Danko, J. C., "Stress Corrosion Cracking and Corrosion Fatigue in Reactor Coolant Piping," Corrosion in Power Generating Equipment, ed. Markus O. Speidel and Andrejs Atrens, Plenum Press, New York, 1984, pp. 233-268.
8. Ford, F. P., "Mechanisms of Stress Corrosion Cracking," Aspects of Fracture Mechanics in Pressure Vessels and Piping, PVP-Vol. 58, ASME, New York, 1982, pp. 229-269.

9. Ford, F. P., Mechanisms of Environmental Cracking in Systems Peculiar to the Power Generation Industry, EPRI NP-2589, General Electric Company Report, Sept. 1982.

10. Mowbray, D. F., "Derivation of a Low-cycle Fatigue Relationship Employing the J-Integral Approach to Crack Growth," Cracks and Fracture, ASTM STP 601, ASTM, Philadelphia, 1976, pp. 33-46 .

11. Begley, J. A., Landes, J. D., and Wilson, W. K., "An Estimation Model for the Application of the J-Integral," Fracture Analysis, Part II, ASTM STP 560, ASTM, Philadelphia, 1976, pp. 155-169.

12. Bucci, R. J., Paris, P. C., Landes, J. D., and Rice, J. R., "J-Integral Estimation Procedures," Fracture Toughness, Part II, ASTM STP 514, ASTM, Philadelphia, 1972, pp. 40-69.

13. Maiya, P. S., and Shack, W. J., "Effects of Nominal and Crack-Tip Strain Rate on IGSCC Susceptibility in CERT Tests," Embrittlement by the Localized Crack Environment (Proc. ASM Intl. Symposium, Philadelphia, PA, October 4-5, 1983), ed. R. P. Gangloff, American Institute of Mining, Metallurgical, and Petroleum Engineers, Inc., New York, 1984, pp. 199-209.

14. Maiya, P. S., "Quantitative Description of Strain Rate Effects on Susceptibility to Intergranular Stress Corrosion Cracking," Advances in Fracture Research, (Proc. 6th Intl. Conf. on Fracture, New Delhi, India, December 4-10, 1984), ed. S. R. Valluri, D. M. R. Taplin, P. Rama Rao, J. F. Knott, and R. Dubey, Pergamon Press, New York, 1984, Vol. 4, pp. 2335-2343.

15. Garud, Y. S., and Gerber, T. L., "Development of an Engineering Model for Predicting IGSCC Damage-Particularly in BWR Water Environments," EPRI NP-2808-LD Project T118-12-2, Topical Report, Feb. 1983.

16. Maiya, P. S., and Shack, W. J., "Evaluation of Nonenvironmental Corrective Actions," Light-Water-Reactor Safety Materials Engineering Research Programs: Annual Progress Report, October 1983-September 1984, in preparation; also presented at Corrosion 85, sponsored by N.A.C.E., Boston, MA, March 25-29, 1985.

17. Ruther, W. E., Soppet, W. K., Ayrault, G., and Kassner, T. F., "Effect of Sulfuric Acid, Oxygen, and Hydrogen in High Temperature Water on Stress Corrosion Cracking of Sensitized AISI 304 Stainless Steel," Corrosion, Vol. 40, No. 10, 1984, pp. 518-527.

18. Clarke, W. L., The EPR Method for the Detection of Sensitization in Stainless Steels, NUREG/CR-1095, GEAP-24-888, Nuclear Engineering Division, General Electric Company, San Jose, CA, 1981.

19. Ruther, W. E., Soppet, W. K., and Kassner, T. F., "Evaluation of Environmental Corrective Actions," Materials Science and Technology Division Light-Water-Reactor Safety Research Program: Quarterly Progress Report, October-December 1983, NUREG/CR-3689 Vol. IV, ANL-83-85 Vol. IV, August 1984.

Table 1. Chemical Composition (wt.%) of Stainless Steels Considered in the Present Study

Material	Heat No.	C	Mn	P	S	Si	Ni	Cr	Mo	Co	Cu	N	O	B	Fe
316	0590019	0.05	1.68	0.030	0.008	0.71	10.83	17.34	2.05	0.34	0.20	0.0145	0.0011	0.0005	Balance
316NG	P91576	0.015	1.63	0.020	0.010	0.42	10.95	16.42	2.14	-	-	0.068	-	0.002	Balance
304	30956	0.06	1.54	0.019	0.007	0.48	8.00	18.99	0.44	0.10	0.19	0.10	-	-	Balance

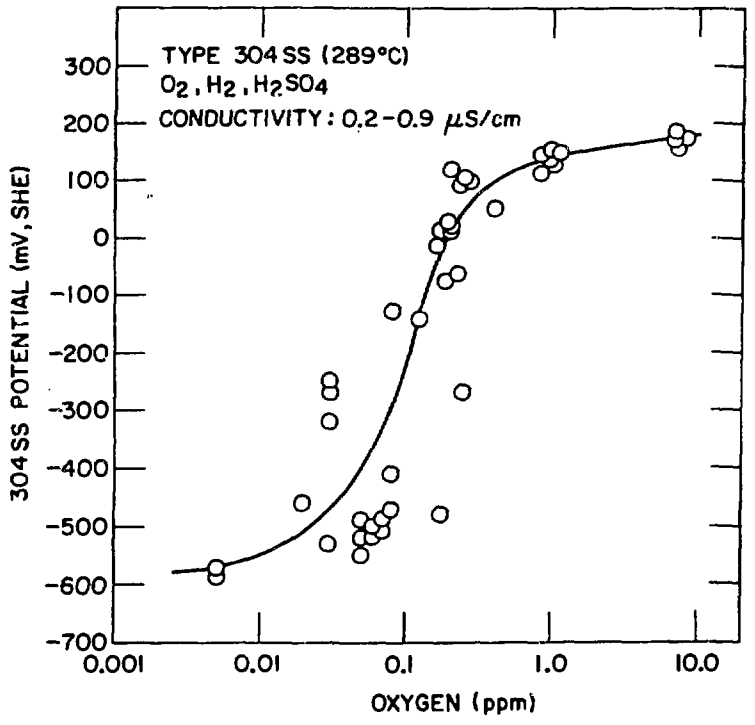

Fig. 1. Variation of Steady-State Open-Circuit Corrosion Potential of Type 304 SS with Dissolved-Oxygen Concentration in an Impurity Environment during CERT Tests at 289°C.

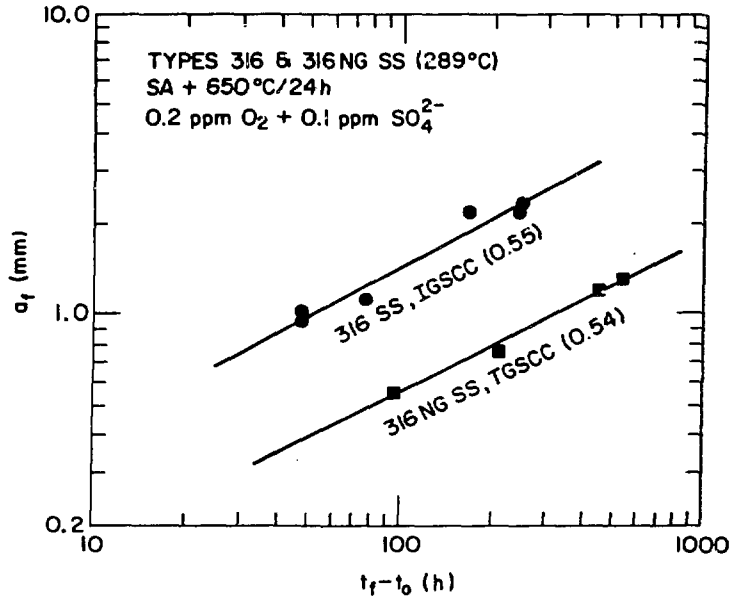

Fig. 2. Correlation between Crack Length at Failure (a_f) and Time to Failure (Corrected for Crack Initiation Time) in Tests Conducted at Different Strain Rates.

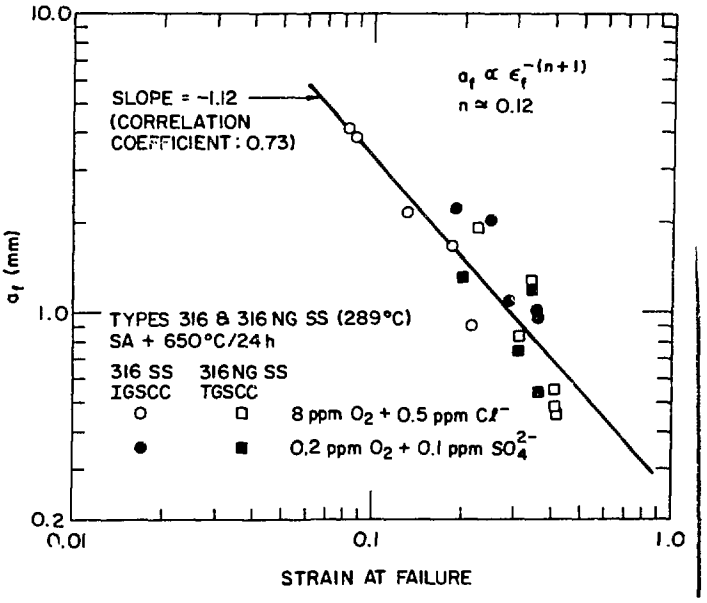

Fig. 3. Correlation between Crack Length at Failure (a_f) and Strain at Failure (ε_f) in Tests Conducted in Two Environments.

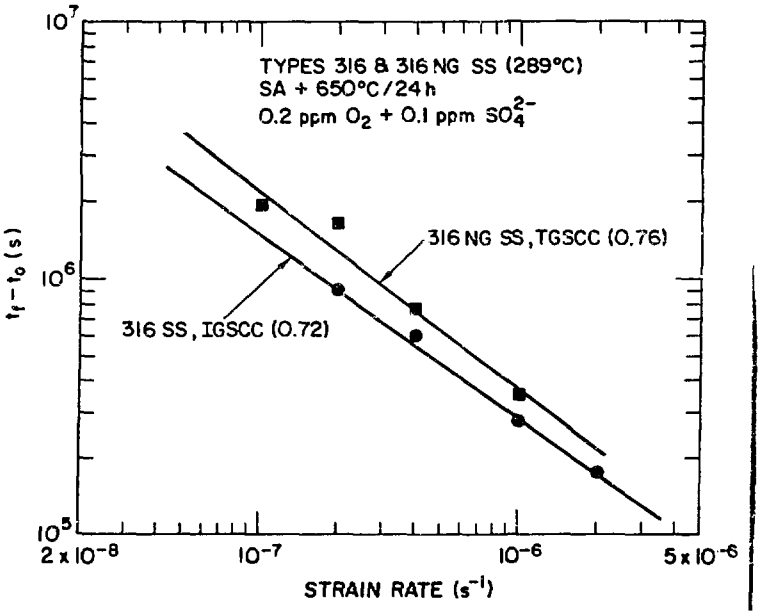

Fig. 4. Correlation between Time to Failure and Strain Rate for Failure by IGSCC and TGSCC.

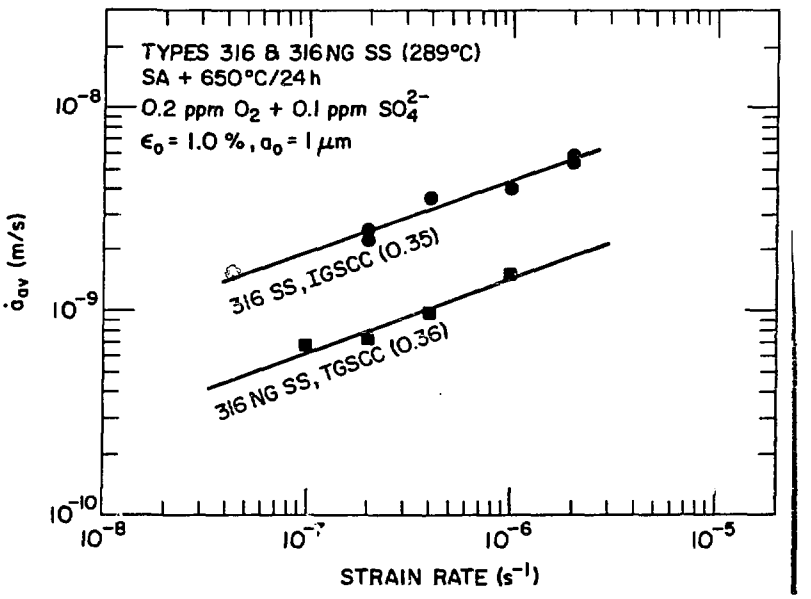

Fig. 5. Effects of Strain Rate on Average Crack Growth Rates for Types 316 and 316NG SS in a Sulfate Environment.

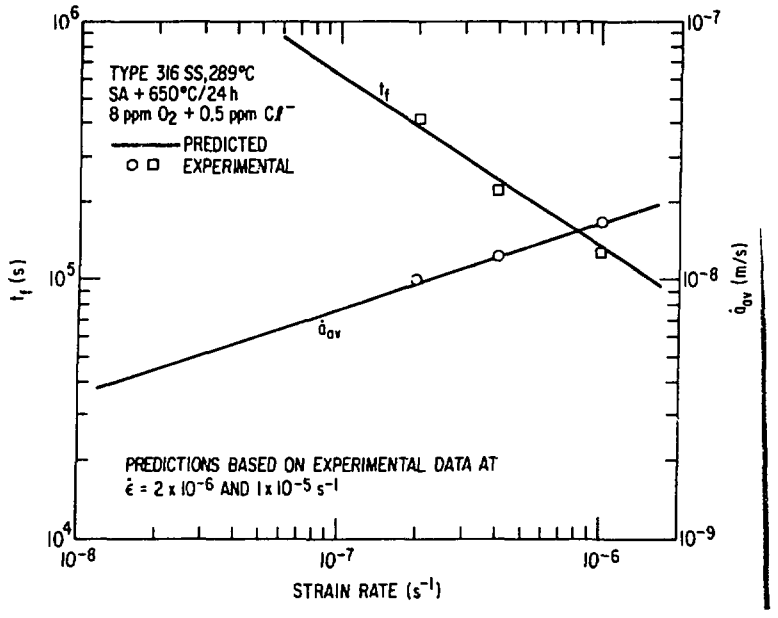

Fig. 6. Extrapolation of IGSCC Susceptibility from High Strain Rates to the Slower Strain Rate Regime. Data are taken from Ref. 14.

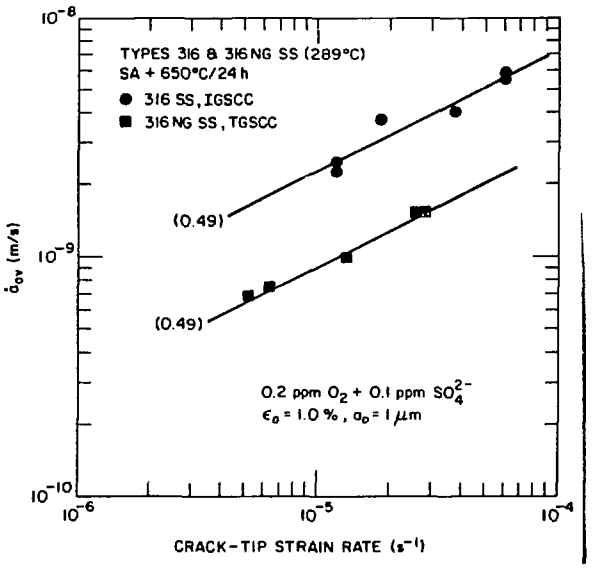

Fig. 7. Relationship between Nominal Strain Rate and Average Near-Crack-Tip Strain Rate for Types 316 and 316NG SS in a Sulfate Environment.

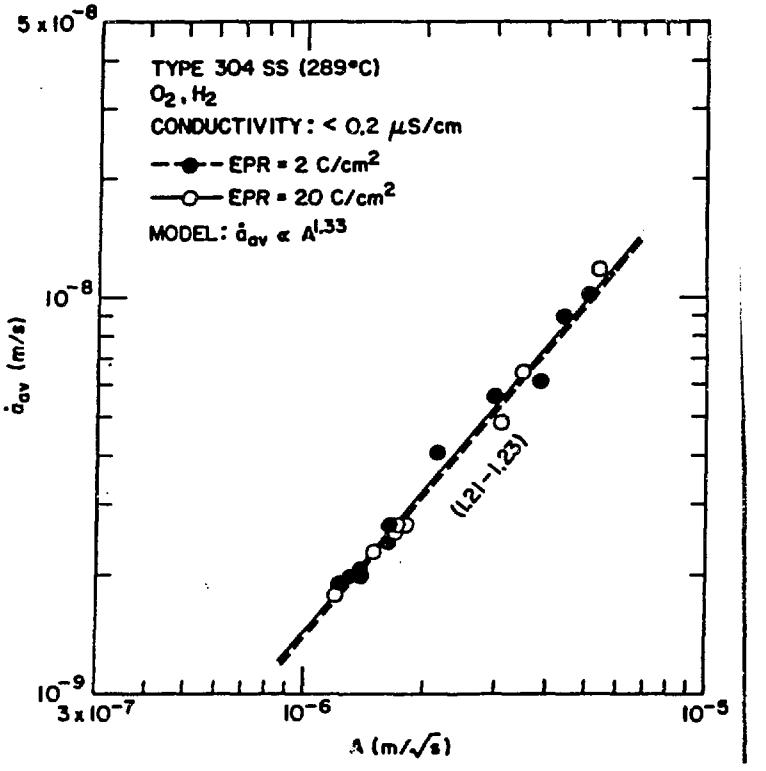

Fig. 8. Variation of Average Crack Growth Rate with the Model Crack Growth Parameter ($A = a_f t_f^{-0.5}$) for Sensitized Type 304 SS in High-Purity Water Containing Different Concentrations of Dissolved Oxygen.

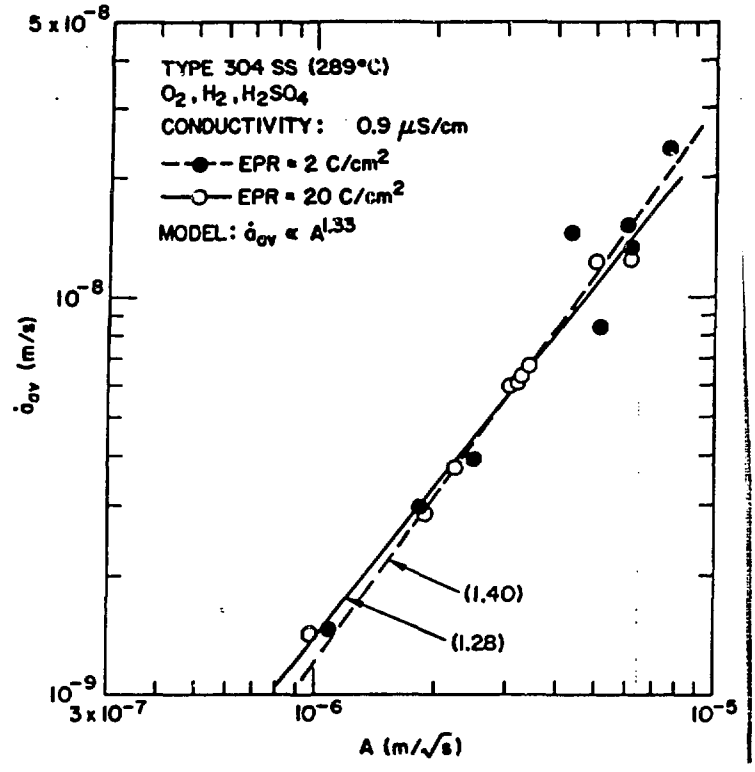

Fig. 9. Variation of Average Crack Growth Rate with the Model Crack Growth Parameter ($A = a_f t_f^{-0.5}$) for Sensitized Type 304 SS in Sulfate Environments Containing Different Concentrations of Dissolved Oxygen.

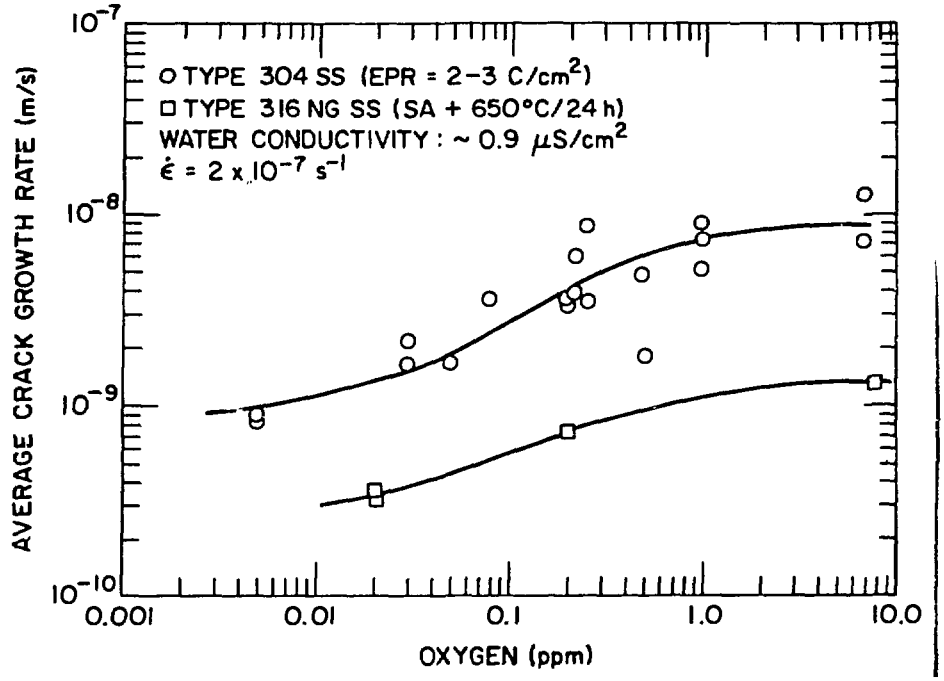

Fig. 10. Effects of Dissolved Oxygen on Average Crack Growth Rates for Types 304 and 316NG SS in an Impurity Environment. The curve for Type 304 SS was deduced from data obtained at $\dot{\varepsilon} = 1 \times 10^{-6}$ s^{-1} (Ref. 19).